Compressive Sensing on Three Dimensional SFCW Ground-Penetrating Radar

Jon Álvarez Justo, Egil Eide, Milica Orlandić
Department of Electronic Systems
Norwegian University of Science and Technology (NTNU)
Trondheim, Norway
jonalv@stud.ntnu.no, egil.eide@ntnu.no, milica.orlandic@ntnu.no

***Abstract*—Stepped-frequency continuous-wave ground-penetrating radars (SFCW GPRs) are characterized by relatively low data acquisition speed caused by stepwise slow scanning of the frequency spectrum. The improvement of the imaging speed in SFCW GPR mostly relies on reducing the data acquisition time. In this paper, a paradigm of compressive sensing (CS) is explored in order to minimize the acquisition time in three dimensional SFCW GPRs by reducing the amount of real-time acquired data below the Nyquist rate by the use of the likely spatial sparsity of the underground. The signal reconstruction is performed by using the greedy algorithm Orthogonal Matching Pursuit (OMP). Data set with synthetic underground mines is accurately reconstructed for compression ratios up to 85% causing that the data acquisition time is reduced 6.67 times. In addition, the results show that for the data set of synthetic mines degraded by uniform noise, the proposed CS approach can be used for effective noise-removal filtering.**

***Index Terms*—Compressive Sensing (CS), Orthogonal Matching Pursuit (OMP), Nyquist rate, sparsity, Stepped-Frequency Continuous-Wave Ground-Penetrating Radar (SFCW GPR)**

I. Introduction

Radar systems transmit microwave electromagnetic radiation pulses which are reflected by the objects on their path. In pulsed radars, the time between pulses and their reflected components is used to determine the distance between the radar and the observed objects. A Ground-Penetrating Radar (GPR) performs detection and imaging of the underground targets based on the reflected signal. GPR has been extensively used as an effective non-destructive technology for a wide range of applications such as detection of pipes, cables and other subsurface infrastructures. The image produced by GPR containing information in form of reflections of the underground targets is known as *radargram*. The Stepped-Frequency Continuous-Wave (SFCW) GPR system synthesizes pulses in frequency domain instead of in time domain. An SFCW radar transmits ideally all frequency components in a stepwise manner within a defined bandwidth contained in one corresponding time domain impulse. The quality of synthesized impulses is determined by the number of frequencies and in this manner, the accuracy of the object imaging can be increased compared to other radar types. This comes at the cost of low scanning speed since the time needed to acquire data over the radar bandwidth is excessively high [1]. A possible approach to reduce the acquisition time is by acquiring less frequency components or by transmitting simultaneously a number of frequencies. Simultaneous transmission increases the complexity of hardware and introduces radio-frequency coupling problems, whereas lowering the number of frequency components leads usually to the ambiguity phenomena in the reconstructed signal. In the literature, the use of a novel digital signal processing technique known as Compressive Sensing (CS) to reduce the amount of real-time acquired data is introduced [1], [2]. The CS approach reconstructs a signal without aliasing for sampling rates below the Nyquist rate with the requirement for the acquired signal to be sparse in a particular basis. A signal is considered sparse in a domain if it can be represented by a few significant nonzero coefficients, whereas the remaining coefficients are equal to zero. Fortunately, most of real-applications signals are either sparse or almost sparse. Indeed, in GPR applications, the underground space is usually almost sparse as the number of targets is likely to be far below the total number of spatial positions [1]. In addition to the sparsity requirement, the data sampling must be incoherent which is ensured by performing the sampling randomly. Although CS data acquisition is less demanding, the signal reconstruction achieved by means of sparse recovery algorithms requires high computational resources.

The remainder of the paper is organized as follows. Section II reviews the principles of CS and the sparse recovery algorithms. In Section III, a feasibility study of CS in a three dimensional SFCW GPR is performed and an implementation of a compressive SFCW GPR system is presented. Section IV describes the results of experiments with simulated underground mines obtained with and without uniform noise. Finally, Section V summarizes the main conclusions and suggests the future work.

II. Background

A. Principles of compressive sensing (CS)

Let vector $\mathbf{f}$ contain N samples acquired at the Nyquist rate in a certain domain. The transform matrix $\mathbf{\Psi}_{NxN}$ is used to transform a signal between different domains. For instance, the *Discrete Fourier Transform* (DFT), *Discrete Cosine Transform* (DCT), and *Discrete Wavelet Transform* (DWT) matrices are frequently used as $\mathbf{\Psi}$ in various applications. The acquired

samples in $\mathbf{f}$ can be represented as a linear combination of the orthogonal basis vectors [3]:

$$\mathbf{f} = \mathbf{\Psi x}, \tag{1}$$

where $\mathbf{x}$ is the vector in transform domain with length N.
In CS, measurement vector $\mathbf{y}$ with M elements is collected by computing the randomized projections of $\mathbf{f}$ over the measurement matrix $\mathbf{\Phi}$ of size $M \times N$ as given:

$$\mathbf{y} = \mathbf{\Phi f} = \mathbf{Ax}, \tag{2}$$

where $\mathbf{A}$ is the dictionary given by the matrix product of $\mathbf{\Phi}$ and $\mathbf{\Psi}$. This is an undetermined system of linear equations with either no solution or infinitely many solutions since the number of unknowns N is greater than the number of equations M. This problem is simplified if $\mathbf{x}$ is a sparse signal, i.e., most of its coefficients are zero and only a few are different from zero. The *support* of vector $\mathbf{x}$ is defined as a set of indexes of the nonzero coefficients [3]:

$$supp(\mathbf{x}) = \{n \in [1, N] \mid x[n] \neq 0\}, \tag{3}$$

and the *sparsity level* K of $\mathbf{x}$ is defined as its number of nonzero coefficients:

$$K = card\{supp(\mathbf{x})\}. \tag{4}$$

For a K-sparse signal $\mathbf{x}$ when $K \ll N$, sparse recovery algorithms can be used to encounter an accurate approximation of the unique solution of the proposed system of equations. In addition, the incoherence property for $\mathbf{\Phi}$ with $\mathbf{\Psi}$ is ensured by performing the sampling randomly as any transform matrix $\mathbf{\Psi}$ is highly probable to be incoherent with randomly built measurement matrix $\mathbf{\Phi}$ [4]. In the light of this, there are different manners to build the randomness of $\mathbf{\Phi}$ [3]. In this paper, it is obtained by:

1) generating a random vector $\boldsymbol{\gamma}$ of length M which contains the randomly chosen indexes in vector $\mathbf{f}$,
2) building an $M \times N$ matrix $\mathbf{0}$ with elements equal to zero,
3) and setting to one the matrix element in each correspondent row of $\mathbf{0}$ whose column index equals to the index of the element taken from vector $\mathbf{f}$ as follows:

$$\mathbf{\Phi} = \mathbf{0}_{(j,\gamma_{(j,1)})_{1 \leq j \leq M}} = 1. \tag{5}$$

Consequently, the dictionary $\mathbf{A}$ corresponds to a *partial random transform matrix* since $\mathbf{A}$ contains only rows of matrix $\mathbf{\Psi}$ which correspond to the coefficient indexes taken from $\mathbf{f}$. This can be expressed as follows:

$$\mathbf{A} = \mathbf{\Psi}_{(\gamma_{(j,1)},\forall)_{1 \leq j \leq M}}. \tag{6}$$

Finally, the *Compression Ratio* denoted as CR, measures how much the data is to be compressed compared to the amount of data acquired at the Nyquist rate. The CR is given as:

$$CR\,(\%) \;=\; (1 - \frac{M}{N}) \;\cdot\; 100. \tag{7}$$

B. False alarms ratio accuracy metric

If the recovery provided by the sparse recovery algorithms is not accurate enough, the estimation of $\mathbf{x}$ might contain undesired false alarms from non-existent underground targets. An estimation accuracy metric *false alarms ratio (FAR)*, is given as follows:

$$FAR\,(\%) \;=\; \frac{False\ alarms}{Total\ detected\ targets} \;\cdot\; 100, \tag{8}$$

where the *total detected targets* term corresponds to the number of estimated significant coefficients whilst the *false alarms* is defined as the number of significant coefficients which are surrounded by nonsignificant pixels equal to zero as depicted in Fig. 1.

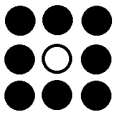

Figure 1: A nonzero pixel (white) surrounded by nonsignificant pixels (black)

The presented accuracy metric is based on the assumption that underground targets are represented in radargrams in the form of hyperbolas and therefore isolated one-pixel targets are registered as false alarms.

C. Overview of sparse recovery algorithms

Sparse recovery algorithms estimate a unique sparse solution to the system in (2). Although each algorithm approaches the problem differently, the common goal is to estimate the nonzero coefficients values in $\mathbf{x}$ as well as their respective indexes. The algorithms are usually classified in two main groups, convex optimization and greedy algorithms, depending on their reconstruction accuracy and computational complexity [5]. The convex optimization algorithms, such as *Basis Pursuit* (BP) [6] and *Gradient Projection for Sparse Reconstruction* (GPSR) [7], provide accurate reconstruction at the expense of high computational complexity. On the other side, greedy algorithms include pursuit and thresholding algorithms such as *Matching Pursuit* (MP) [8], *Orthogonal Matching Pursuit* (OMP) [9], *Compressive Sampling Matching Pursuit* (CoSaMP) [10], *Regularized Orthogonal Matching Pursuit* (ROMP) [11], and *Iterative Hard Thresholding* (IHT) [12] which offer relatively low computational complexity at the expense of reducing the estimation accuracy.

D. Orthogonal Matching Pursuit (OMP)

OMP [13] is an iterative algorithm widely used for sparse recovery due to its moderate simplicity, and acceptable accuracy. The iteration i of the algorithm is depicted in Fig. 2.

Estimation of the index of a new nonzero coefficient in $\mathbf{x}$ is performed by analyzing which atom $\mathbf{a}$, a column in the dictionary $\mathbf{A}$, presents the highest projection over the residue $\mathbf{r^{(i-1)}}$ computed in the previous iteration (for i=1, $\mathbf{r^{(i-1)}}$=$\mathbf{y}$).

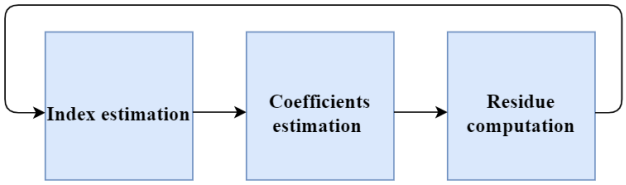

Figure 2: Computational steps in one iteration of OMP algorithm

The index of the highest projection in magnitude, $\lambda^{(i)}$, given as:

$$\lambda^{(i)} = argmax(\begin{bmatrix} | \langle \mathbf{a_1}, \mathbf{r^{(i-1)}} \rangle | \\ | \langle \mathbf{a_2}, \mathbf{r^{(i-1)}} \rangle | \\ \vdots \\ | \langle \mathbf{a_N}, \mathbf{r^{(i-1)}} \rangle | \end{bmatrix}) \tag{9}$$

matches not only the index of the maximum correlation atom $\mathbf{a}_{\lambda^{(i)}}$, but also the index of the new significant coefficient to estimate. The computed $\lambda^{(i)}$ is added to vector $\hat{\mathbf{c}}^{(\mathbf{i})}_{\mathbf{i}\times\mathbf{1}}$ which collects the indexes of the nonzero coefficients calculated in the different iterations. The atom $\mathbf{a}_{\lambda^{(i)}}$ is added to an augmented subdictionary $\mathbf{B}^{(\mathbf{i})}_{\mathbf{M}\times\mathbf{i}}$ which gathers the highest projection atoms selected across the iterations.

Estimation of the new nonzero coefficient $\hat{x}_{(\lambda^{(i)},1)}$, and tuning of the coefficients computed in the previous iterations is done by computing the projections over the subdictionary $\mathbf{B}^{(\mathbf{i})}$ as follows:

$$\mathbf{y} = \mathbf{B}^{(\mathbf{i})}\mathbf{s}^{(\mathbf{i})}, \tag{10}$$

where $\mathbf{s}^{(\mathbf{i})}_{\mathbf{i}\times\mathbf{1}}$ contains the values of the nonzero coefficients computed up to the current iteration. To ensure a unique solution, the *least squares* (LS) criterion is used to approximate $\mathbf{s}^{(\mathbf{i})}$ as follows:

$$\hat{\mathbf{s}}^{(\mathbf{i})} = (\mathbf{B}^{(\mathbf{i})^{\mathbf{T}}}\mathbf{B}^{(\mathbf{i})})^{-1}\mathbf{B}^{(\mathbf{i})^{\mathbf{T}}}\mathbf{y} \tag{11}$$

s.t.

$$\min(|| \mathbf{y} - \mathbf{B}^{(\mathbf{i})}\hat{\mathbf{s}}^{(\mathbf{i})} ||_2^2). \tag{12}$$

Residue computation to determine the estimation error is given as:

$$\mathbf{r}^{(\mathbf{i})}_{\mathbf{M}\times\mathbf{1}} = \mathbf{y} - \mathbf{B}^{(\mathbf{i})}\hat{\mathbf{s}}^{(\mathbf{i})}. \tag{13}$$

The orthogonality of the subdictionary atoms over the residue, i.e., $\langle \mathbf{a_j}, \mathbf{r}^{(\mathbf{i})} \rangle = 0$ for $\forall\ \mathbf{a_j} \in \mathbf{B}^{(\mathbf{i})}$, prevents from selecting the same atom in the next iterations.

Once the algorithm halts after a certain stop condition is met in the I-th iteration, the estimation $\hat{\mathbf{x}}$ is obtained by placing the entries from $\hat{\mathbf{s}}^{(\mathbf{i}=\mathbf{I})}_{\mathbf{I}\times\mathbf{1}}$ in the respective indexes given by $\hat{\mathbf{c}}^{(\mathbf{i}=\mathbf{I})}_{\mathbf{I}\times\mathbf{1}}$.

III. Feasibility Study of Compressive Sensing on the SFCW GPR and Proposed Methodology

A. Compressive sensing on the SFCW GPR

The SFCW GPR under study scans the electromagnetic spectrum in the range 30 MHz-3030 MHz [14] by acquiring one frequency sample per step. The system senses the underground in three dimensions by means of the array of transmit and receive antennas shown in Fig. 3. The information is stored in a frequency data cube, shown in Fig. 4, where the X, Y, and Z dimensions correspond, respectively, to the in-line direction, cross-line direction, and the direction perpendicular to the ground. A data set with synthetic underground mines is

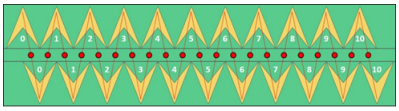

Figure 3: Array of transmit and receive antennas [14]

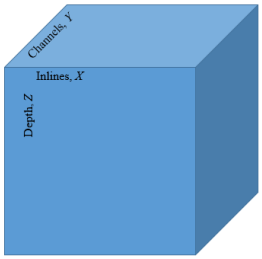

Figure 4: Data cube format for storing the underground data

used to study whether the sparsity requisite is satisfied. Fig. 5 shows the magnitude and phase of the complex received signal in the frequency domain for a given position (X,Y).

While the frequency data are used in some applications to detect and measure the material properties of the subsurface, it does not evince the echoes from the underground targets. However, Fig. 6 shows that after performing the *Inverse Fast Fourier Transform* (IFFT) of the frequency data, the echoes emerge in the resulting complex time domain signal. In particular, the main reflection (at 2.2 ns) is produced by the coupling from the transmit antenna that this system normally presents, and the weaker echo (at 7.9 ns) corresponds to an actual underground target, specifically a mine.

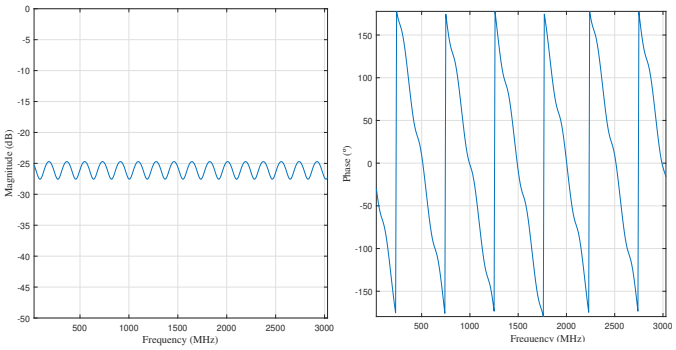

(a) Magnitude (b) Phase

Figure 5: Magnitude and phase of the complex frequency domain signal

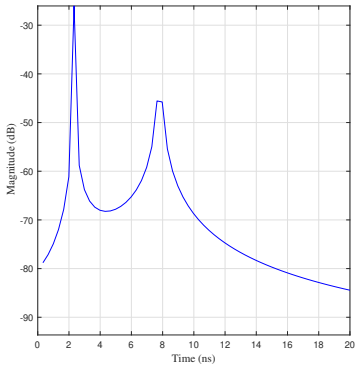

Figure 6: Magnitude of the complex time domain signal

When analyzing the sparsity requirement of the data in the frequency and time domains, neither the frequency nor time data are strictly sparse. Nonetheless, the time domain presents a *compressible* behavior. A signal is considered compressible when most of its coefficients are close to zero (in linear units), and only a few of them (in this case, the reflections) are nonzero. Such signals are often approximated as sparse. Accordingly, it is acceptable that the time domain signal is assumed to be sparse. As a conclusion, for the SFCW GPR under study, CS is a feasible paradigm to compress the acquired data in frequency domain, and perform the sparse recovery in time domain. If the reconstruction is performed with enough accuracy, the recovered time domain signal $\hat{\mathbf{x}}$ should contain only the echoes from the underground targets. Conversely, if the recovery is not accurate enough, *false alarms* might occur in the signal.

B. Sparsity level estimation analysis

A halting criterion needs to be defined to bound the execution time required by the OMP algorithm to perform the signal recovery. Typically, a halting condition consists of either setting a threshold over the maximum reconstruction error or limiting the minimum error difference between iterations. However, assuming that the algorithm chooses correctly in each iteration a new atom in the dictionary $\mathbf{A}$, only K iterations are demanded to reconstruct a K-sparse signal and the total number of iterations may be bounded to K. Due to the fact that $\mathbf{x}$ and K are unknown, an estimate of the sparsity level $\hat{K}$ needs to be provided to the algorithm. The parameter $\hat{K}$ has a direct impact on both computation time and reconstruction accuracy.

For a low $\hat{K}$, the algorithm estimates a sparse $\hat{\mathbf{x}}$ by setting a conservative (high) threshold over the signal to estimate. On the other side, a high $\hat{K}$ gives as a result a dense $\hat{\mathbf{x}}$ by setting a soft (low) threshold. Consequently, a low $\hat{K}$ is more likely to reduce the number of false alarms compared to a high $\hat{K}$. Regarding the compression ratio, the more the data are compressed, i.e., the higher CR, the less accurate reconstruction of the signal is obtained. Indeed, a high CR lowers the number of residue entries which are minimized in each iteration leading to an estimation with increased false alarms.

A trade-off study between $\hat{K}$ and CR for accurate signal reconstruction follows. For high CR, a conservative threshold, i.e., a low $\hat{K}$, needs to be set to diminish the false alarms, whereas both soft and conservative thresholds, i.e., high or low $\hat{K}$ values, can be utilized for low CR. In a reconstruction containing a low number of false alarms for a certain $\hat{K}$ and a medium CR, a decrease of $\hat{K}$ does not raise the number of false alarms, whereas the number of false alarms increases as $\hat{K}$ increases. The false alarms due to the increase of $\hat{K}$ can be lowered by reducing the CR. For estimating the underground sparsity, a previous knowledge about the underground is important. However, with no prior information about $\hat{K}$, the trade-off study can be used for parameter tuning in the reconstruction process. The lower occurrence of false alarms in the beginning of the reconstruction process is ensured by setting low CR and $\hat{K}$ parameters. The two parameters can be then tuned accordingly to obtain the desired sparsity and compression.

Finally, the time required for the reconstruction is also a relevant aspect for real-time data recovery in GPR technology. The reconstruction time depends on both $\hat{K}$ and CR, having $\hat{K}$ the greater impact on the total time as it directly sets the halting condition of the algorithm.

C. Proposed methodology

The implementation of a compressive SFCW GPR system is performed in MATLAB. As shown in Fig. 7, it comprises two modules:

- Random subsampling module with vector $\mathbf{f}$ containing N frequency samples and CR parameter as inputs. The module generates vector $\boldsymbol{\gamma}$ with random indexes and outputs the randomly subsampled frequency data $\mathbf{y}$ and the dictionary matrix $\mathbf{A}$ built as a partial random Fourier matrix according to $\boldsymbol{\gamma}$.
- OMP module contains as inputs the estimated sparsity level $\hat{K}$ in addition to vector $\mathbf{y}$ and matrix $\mathbf{A}$. Its outputs are the estimated time domain signal $\hat{\mathbf{x}}$ and the error of the estimation $\mathbf{r}^{(\mathbf{i}=\hat{\mathbf{K}})}$.

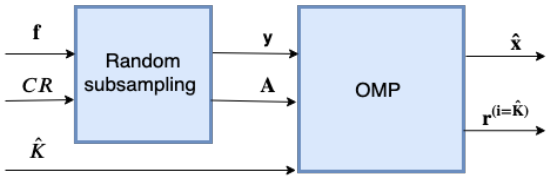

Figure 7: Modules of the compressive SFCW GPR

IV. Results

A. Estimated noise-free radargrams

Original and estimated XZ radargrams are computed from $|\mathbf{x}|$ and $|\hat{\mathbf{x}}|$, respectively. A characteristic channel Y with clear underground mines has been selected in the results below.

Fig. 8 shows the original radargram where each hyperbola corresponds to a different underground mine. There are two shallow side mines, a deep mine in between and the coupling from the transmit antenna translated into a shallow horizontal line.

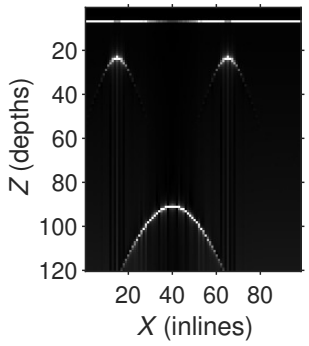

Figure 8: Original radargram

The estimated radargram in Fig. 9a is the result of OMP algorithm for $\hat{K}$=5 and CR=85%. When compared with the original radargram, the algorithm is capable of:

- estimating inlines with echoes in $\mathbf{x}$ corresponding to the reflections from the mines as well as the transmit coupling,
- estimating the placement of the significant samples in $\mathbf{x}$,
- suppressing the nonsignificant samples in $\mathbf{x}$.

Accurate estimation of the placement of significant samples in $\mathbf{x}$ implies that the targets are estimated at the right depths. Fig. 9b shows the estimated radargram for $\hat{K}$=25 and CR=85%. In this case, the hyperbolas have more defined shapes in comparison to Fig. 9a due to the denser $\hat{\mathbf{x}}$. However, it confirms that a higher $\hat{K}$ leads to a soft threshold which raises the number of false alarms from FAR=2.50% (Fig. 9a) to 32.73% (Fig. 9b) when the CR is also high. The high density of $\hat{\mathbf{x}}$ in Fig. 9b can be maintained without paying the price of false alarms if the CR is reduced to 50%, as shown in Fig. 9c. Since the low CR increases the number of residues minimized in each iteration, the false alarms are considerably diminished to FAR=1.56%. As a conclusion, the low $\hat{K}$ values can be selected along with either high or low CR values, but higher $\hat{K}$ values are only to be used combined with low CR values. In addition, Fig. 9c shows that the estimated radargram presents pixels with similar colour to the pixels in the original radargram in Fig. 8. In short, the algorithm is able to estimate accurately the strength of the received reflections. Under the assumption of uniform sensing time, the time required for CS data acquisition with compression ratio $CR = 85\%$ is $\approx$ 6.67$\times$ lower than the time used for obtaining uncompressed data. Finally, Fig. 9d shows the estimated radargram for $\hat{K}$=5 and CR=85% when the data sensing is performed periodically. The non-random acquisition leads to an unsuccessful reconstruction with many false alarms (FAR=36.73%) as the incoherence requirement

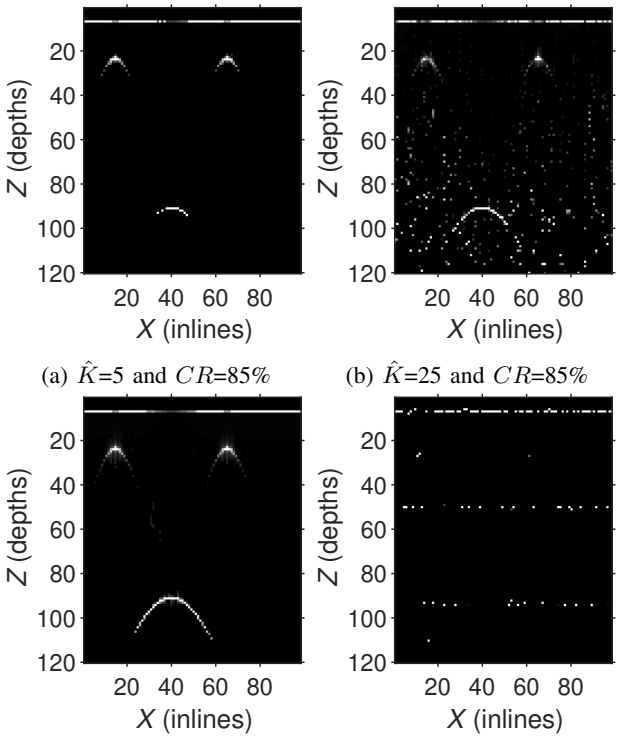

(a) $\hat{K}$=5 and CR=85% (b) $\hat{K}$=25 and CR=85%

(c) $\hat{K}$=25 and CR=50% (d) $\hat{K}$=5 and CR=85%

Figure 9: Estimated radargrams

is not fulfilled. Parameters $\hat{K}$, CR and FAR for the previous noise-free radargrams are summarized in Table I.

TABLE I: Estimation accuracy in noise-free radargrams

$\hat{K}$	CR	FAR	Figure
5	85%	2.50%	9a
5 (periodic)	85%	36.73%	9d
25	85%	32.73%	9b
25	50%	1.56%	9c

B. Estimated noisy radargrams

Uniform noise, distributed as $\sim [0, \frac{max(|\mathbf{f}|)}{PSNR}]$, is added to the real part of the frequency samples in $\mathbf{f}$, where PSNR is the *Peak Signal-to-Noise Ratio* (in linear units) in the frequency domain. For the analysis, the constant PSNR, specifically PSNR=20 dB, is used. The noise added to the frequency data is translated into noise in time domain. Fig. 10 shows the original radargram created from $\mathbf{f}$ with added uniform noise. Fig. 11a shows the estimated radargram computed from the noisy $\mathbf{y}$ for $\hat{K}$=5 and CR=50%. It is shown that the false alarms produced by the noise have been filtered out. As a conclusion, CS can be used for noise-removal filtering. Since noisy scenarios significantly increase the occurrence of false alarms, conservative thresholds, i.e., low $\hat{K}$ values, are used to ensure that most of the false alarms are filtered out. To illustrate this point, Fig. 11b shows the estimated radargram computed from the noisy $\mathbf{y}$ when CR=50% and soft threshold $\hat{K}$=25 is used. The number of false alarms after lowering the

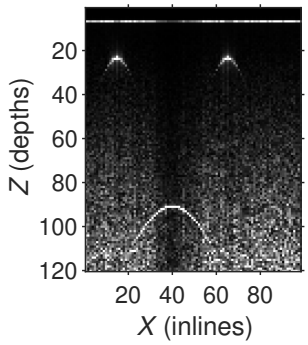

Figure 10: Original radargram from noisy $\mathbf{f}$

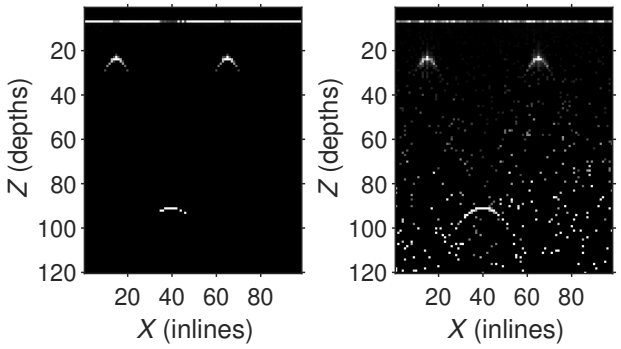

(a) $\hat{K}$=5 and CR=50% (b) $\hat{K}$=25 and CR=50%

Figure 11: Estimated noisy radargrams

threshold to $\hat{K} = 25$ is increased to FAR=37.14% compared to Fig. 11a which presents FAR=1.82%. A reduction of CR does not decrease the occurrence of false alarms as the threshold is not conservative enough. Therefore, the false alarms can only be diminished by lowering $\hat{K}$. Parameters $\hat{K}$, CR and FAR for the previous noisy radargrams are summarized in Table II.

TABLE II: Estimation accuracy in noisy radargrams

$\hat{K}$	CR	FAR	Figure
5	50%	1.82%	11a
25	50%	37.14%	11b

V. Conclusion and further direction

In this paper, the feasibility of using CS sparse recovery algorithms in three dimensional SFCW GPR to decrease the amount of real-time data sensed and thus reduce its acquisition time is discussed. The OMP algorithm is used to recover the synthetic data set of the underground mines with the assistance of an a priori estimate of the underground sparsity. Based on the results, it can be concluded that a low sparsity level sets a conservative threshold reducing the false alarms at the expense of less defined hyperbolas. In addition, low sparsity level values allow the use of both low and high CR values. On the other hand, high sparsity levels give higher accuracy of detection of hyperbolas at the cost of the increased likelihood of false alarm occurrences. In this scenario, it is required that the CR is set to low values to avoid creation of false alarms caused by high CR. The implemented OMP algorithm was verified by the use of a data set with synthetic underground mines, achieving compression ratio CR=85% and potentially reducing in this way the acquisition time by a factor 6.67. Also, the data set reconstruction was successfully tested in the noisy environment by adding uniform noise. It can be concluded that CS can be used for effective noise-removal filtering as long as $\hat{K}$ and CR are properly chosen. The presented work can be further improved by performing CS reconstruction of real data sets.

Acknowledgment

Our special gratitude to Ståle Fjeldstad and Henrik Width from 3D-Radar AS for their continuous support to our work.

References

[1] A. C. Gurbuz, J. H. McClellan and W. R. Scott, "A Compressive Sensing Data Acquisition and Imaging Method for Stepped Frequency GPRs," in IEEE Transactions on Signal Processing, vol. 57, no. 7, pp. 2640-2650, July 2009.

[2] A. B. Suksmono, E. Bharata, A. A. Lestari, A. G. Yarovoy and L. P. Ligthart, "Compressive Stepped-Frequency Continuous-Wave Ground-Penetrating Radar," in IEEE Geoscience and Remote Sensing Letters, vol. 7, no. 4, pp. 665-669, Oct. 2010.

[3] S. Stankovic, I. Orovic, E. Sejdic, "Multimedia Signals and Systems: Basic and Advance Algorithms for Signal Processing," Springer-Verlag, New York, 2015.

[4] R. Karlina, "Compressive sensing applied to high resolution imaging by synthetic aperture radar," Ph.D. dissertation, School Environ. Studies, Tohoku Univ., Sendai, Japan, Aug. 2013

[5] I. Orović, V. Papić, C. Ioana, X. Li, S. Stanković, "Compressive Sensing in Signal Processing: Algorithms and Transform Domain Formulations," Mathem. Problems in Eng., Review paper, 2016.

[6] D. L. Donoho, "Compressed sensing," in IEEE Transactions on Information Theory, vol. 52, no. 4, pp. 1289-1306, April 2006.

[7] M. A. T. Figueiredo, R. D. Nowak and S. J. Wright, "Gradient Projection for Sparse Reconstruction: Application to Compressed Sensing and Other Inverse Problems," in IEEE Journal of Selected Topics in Signal Processing, vol. 1, no. 4, pp. 586-597, Dec. 2007.

[8] S. G. Mallat and Zhifeng Zhang, "Matching pursuits with time-frequency dictionaries," in IEEE Transactions on Signal Processing, vol. 41, no. 12, pp. 3397-3415, Dec. 1993.

[9] Y. C. Pati and R. Rezaiifar and P. S. Krishnaprasad, "Orthogonal matching pursuit: Recursive function approximation with applications to wavelet decomposition," in Conference Record of The Twenty-Seventh Asilomar Conference on Signals, Systems and Computers, 1993.

[10] D. Needell and J. A. Tropp, "Cosamp: Iterative signal recovery from incomplete and inaccurate samples," Appl. Comp. Harmonic Anal., 2008, submitted for publication.

[11] D. Needell and R. Vershynin, "Signal Recovery From Incomplete and Inaccurate Measurements Via Regularized Orthogonal Matching Pursuit," in IEEE Journal of Selected Topics in Signal Processing, vol. 4, no. 2, pp. 310-316, April 2010.

[12] T. Blumensath and M. E. Davies, "Iterative hard thresholding for compressed sensing," Appl. Computat. Harmon. Anal., vol. 27, no. 3, pp. 265–274, Nov. 2009.

[13] Shailesh Kumar, "The OMP Algorithm," https://sparseplex.readthedocs.io/en/latest/book/pursuit/omp/algorithm.html, accessed on 2019.

[14] 3D-Radar AS, "http://3d-radar.com/," accessed on 2019.